

## Ethyne Reducing Metal-Organic Frameworks to Control Fabrications of Core/shell Nanoparticles as Catalysts

Chenghua Zhang,<sup>\*,a,b</sup> Xiaoxue Guo,<sup>b</sup> Qingchun Yuan,<sup>\*,c</sup> Rongle Zhang,<sup>a,b</sup> Qiang Chang,<sup>a,b</sup> Ke Li,<sup>a,b</sup> Bo Xiao,<sup>\*,d</sup> Suyao Liu,<sup>a,b</sup> Caiping Ma,<sup>a,b</sup> Xi Liu,<sup>a,b</sup> Yiqun Xu,<sup>a,b</sup> Xiaodong Wen,<sup>a,b</sup> Yong Yang,<sup>a,b</sup> Yongwang Li<sup>\*,a,b</sup>

<sup>a</sup> State Key Laboratory of Coal Conversion, Institute of Coal Chemistry, Chinese Academy of Sciences, Taiyuan, Shanxi, 030001, P. R. China.

<sup>b</sup> National Energy Center for Coal to Liquids, Synfuels China Co., Ltd., Huairou District, Beijing, 101407, People's Republic of China

<sup>c</sup> Aston Institute of Materials Research, Aston University, Birmingham B4 7ET, the United Kingdom.

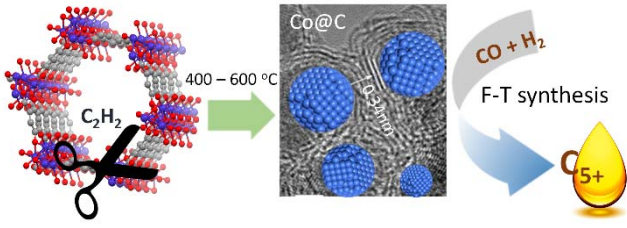
<sup>d</sup> School of Chemistry and Chemical Engineering, Queen's University Belfast, BT9 5AG, the United Kingdom.

### ABSTRACT

An approach using cobalt metal-organic frameworks (Co-MOF) as precursors is established for the fabrication of cobalt nanoparticles in porous carbon shells (core/shell Co@C). Chemical vapor deposition of ethyne is used for controlling the reduction of cobalt nanoclusters in the MOF and the spontaneous formation of the porous carbon shells. The metallic cobalt cores formed are up to 4 - 6 nm with the crystal phase varying between hexagonally-close-packed (*hcp*) and face-centre-packed (*fcc*). The porous carbon shells change from amorphous to graphene with the ethyne deposition temperature increasing from 400 to 600 °C. The core/shell Co@C nanoparticles exhibit high catalytic activity in selectively converting syngas (CTY: 254.1 - 312.1  $\mu\text{molCO}\cdot\text{g}_{\text{Co}}^{-1}\cdot\text{s}^{-1}$ ) into hydrocarbons (4.0 - 5.2  $\text{gHC}\cdot\text{g}\cdot\text{cat}^{-1}\cdot\text{h}^{-1}$ ) at 260 °C. As well as the crystal size and phase, the coordination numbers of the cobalt to oxygen and to other cobalt atoms on the surface of the cobalt nanoparticles, and the permeability of the porous carbon shell have been related to the catalytic performance in FTS reactions.

**Keywords:** Metal-organic-framework, catalysts, chemical vapour deposition, cobalt nanoparticles in carbon, surface chemistry, Fischer-Tropsch synthesis

## Table of Content Graphic



## 1. Introduction

Research interests in metal-organic frameworks (MOFs) have undergone exponential growth over the past decade, which has led to many attractive applications.<sup>1-6</sup> The MOFs contain single metal atoms or nanoclusters in the framework that are orderly separated by organic ligands in a coordinated manner. An extended network is hence built with diverse pore structures and surface functionalities that are tailorable for promoting catalysis, gas adsorption and medicine delivery.<sup>2,3</sup> The formulation of MOF-based catalysts is especially interested here, which can be classified into two categories. The first directly uses the integral structure of MOFs, which has been widely reported.<sup>4-6</sup> The catalytic site is either the metal sites, functional groups of organic ligands, foreign active sites introduced in the pores by post modification or their combination. The second is to convert the well-separated metal nanoclusters in the MOFs to fabricate new structural metal or metal oxide nanoparticles as catalysts or other type of functional materials.<sup>7-15</sup> This fresh emerging route sacrifices the MOF structures.

By sacrificing different types of MOFs such as Fe-BTC,<sup>7,8</sup> ZIF-67,<sup>12,13</sup> and MOF-5,<sup>15</sup> -71<sup>9</sup> and -74,<sup>10,11</sup> the metal nanoparticles of Fe,<sup>7,8</sup> Co<sup>9-13</sup> and Pd<sup>14,15</sup> have been prepared. They are popular active sites for heterogeneous catalysis, for example, cobalt ones (Co<sup>0</sup>) for Fischer-Tropsch synthesis (FTS). The Co<sup>0</sup> nanoparticles supported by carbon or silica have been prepared from Co-containing MOFs such as MOF-71,<sup>9</sup> Co-MOF-74<sup>10</sup> and ZIF-67<sup>12</sup> by direct pyrolysis. As the FTS catalysts they showed very competitive activity and selectivity. The Co<sup>0</sup> nanoparticles in *fcc* phase supported by amorphous carbon showed a C<sub>5+</sub> space-time yield of 0.77 g g-cat<sup>-1</sup>h<sup>-1</sup> at 300 °C and 3.0 MPa.<sup>9</sup> By doping with Si species, the Co nanoparticles were partially transformed into *hcp* phase via a CoC intermediate and showed an C<sub>5+</sub> space-time yield of 1.45 g g-cat<sup>-1</sup>h<sup>-1</sup>, which is higher than that from conventional Co catalysts.<sup>9</sup>

The factors of Co<sup>0</sup> nanoparticles such as surface chemistry, energy and active site population on the surface impact the catalyst performance in the FTS catalysis,<sup>16</sup> among which surface chemistry and energy are not only determined by crystal phases and facets but also by their size and their interaction with the carrier.<sup>17</sup> Dispersing Co<sup>0</sup> nanoparticles to increase active sites and catalytic activity has been a long standing challenge,<sup>18</sup> so does fully reducing cobalt species into metallic cobalt nanoparticles for efficient utilization of the noble metal.<sup>12</sup> Porous inorganic materials built from silica, alumina, titania and zirconia are commonly used to carry metal nanoparticles through impregnation in their salt solutions. However, metal species can readily react with these carrier materials in the catalyst processing (drying, calcining and reducing) to form complex compounds such as cobalt silicates and aluminates in Fischer-Tropsch catalysts<sup>19,20</sup> which are difficult to be reduced and have little activity. This complexity restricts the study of catalytic mechanisms and is a threshold for the development of more efficient catalysts. MOFs as precursors has shown better outcomes than its counterpart of inorganic salts.<sup>12</sup> Condensing silica in the pore space of Co-containing MOF not only generate highly loaded cobalt nanocomposites (~ 50 wt % Co), but also cause a high reducibility of cobalt oxide (up to 80 %) with a good Co<sup>0</sup> nanoparticle distribution (8 - 14 nm). This type of cobalt catalysts exhibits good activity (CTY 78 μmolCO·g<sub>Co</sub><sup>-1</sup>·s<sup>-1</sup>) and high C<sub>5+</sub> selectivity (85 %) at 210 °C and 26 bar.<sup>12</sup> Theoretically, the smaller the metal nanoparticles, the larger the surface energy, and the higher the activity.<sup>20-21</sup> The smaller metal nanoparticles also give rise to better dispersion for more active sites. However, the FTS catalysis is very sensitive to the Co<sup>0</sup>

nanoparticle size. When the  $\text{Co}^0$  nanoparticle is smaller than a critical size, the FTS site activity and the chain growth probability increase with the particle size until reaching a maximum.<sup>18,22-25</sup> Above that, the catalytic activity remains the same approximately. The critical size reported is about 5 - 6<sup>18,22,23</sup> or 10 nm,<sup>12,24-25</sup> depending on the catalyst preparation and reaction conditions. It has been suggested that CO dissociation occurs more easily on larger Co nanoparticles.<sup>26</sup> Small cobalt nanoparticles normally possess a larger fraction of low-coordinated surface sites (i.e. corner, kink and edge), which tend to irreversibly bond CO molecules and hence block part of the cobalt active surface.<sup>18-26</sup> This blocking hampers CO dissociation and/or  $\text{CH}_x$  hydrogenation.

This paper reports our recent development in the precisely-controlled manufacture of ultra-small  $\text{Co}^0$  nanoparticles in porous carbon shells (core/shell  $\text{Co}@C$ ) from Co-containing MOFs. Such core/shell structures were achieved by chemical vapour deposition of ethyne over MOFs. Ethyne deposition has been well studied for the preparation of carbon nanotubes or the carbon-encapsulated metal particles which also called metal@carbon-onions.<sup>27-32</sup> The previous studies focused on the graphitization of carbon materials. The metal nanoparticles in metal@carbon-onions have a broad size distribution varying from 10 to hundreds of nanometers and a low metal concentration. More particularly, the graphitized carbon shells are not porous to chemical reactants, which makes the surface of metal nanoparticles difficult to access and is not ideal for heterogeneous catalysis in FTS. This research aims at the demonstration of a new method for producing uniform, stable and active metal nanoparticles with a small size from MOFs, by which we expect that the cobalt nanoclusters in the Co-MOF selected are reduced by the hydrogen released from ethyne in a precisely controllable manner. The reduced cobalt nanoparticles, smaller than the critical sizes reported, are simultaneously encapsulated by the carbon rejected from ethyne decomposition to form the core/shell  $\text{Co}@C$  nanoparticles, which have a porous carbon shell to facilitate selectively converting syngas into hydrocarbons.

## 2. Experimental

### 2.1 Chemicals and Co-MOF synthesis

A typical Co-MOF ( $\text{Co}_2(\text{dhtp})(\text{H}_2\text{O})_2 \cdot x\text{H}_2\text{O}$ ; *dhtp*: 2,5-dihydroxy-terephthalate; also called CPO-27- $\text{Co}$ <sup>33</sup> or Co-MOF-74<sup>34</sup>) was selected for this FTS study. Cobalt acetate (> 99 %, Sigma Aldrich, UK or Sinopharm Chemical Reagent Co. Ltd.) and 2,5-dihydroxy-terephthalic acid (> 98 %, Hangzhou Sage Chemical Co. Ltd. and TCI (Shanghai) Development Co. Ltd) were used in the synthesis of the Co-MOF. In a typical synthesis, a solution of cobalt acetate (0.373 g, 1.5 mmol) in deionized water (10 mL) and a solution of 2,5-dihydroxyterephthalic acid (0.149 g, 0.75 mmol) in THF (10 mL) were mixed and sealed in a Teflon-lined steel autoclave of 50 mL. The autoclave was kept in an oven where the temperature was maintained at 110 °C for 72 hours. The Co-MOF formed was filtrated and repeatedly washed for characterization and catalysis applications. The solvent Tetrahydrofuran in HPLC grade was from Sigma-Aldrich, UK and Sinopharm Chemical Reagent Co., Ltd.

### 2.2 Chemical vapour deposition and Fischer-Tropsch catalysis tests

Chemical vapour deposition and FTS tests were performed continuously in stainless steel fixed-bed reactors.

The beds have an inner diameter of 6 - 12 mm. Typically, a Co-MOF sample of 1.0 ml was packed in the isothermal region of the reactor. The remaining volume was filled with quartz granules of 80 - 100 mesh. The chemical vapour deposition of ethyne on the Co-MOF was carried out in the flow of 2.0 % C<sub>2</sub>H<sub>2</sub> in Helium (50 ml min<sup>-1</sup>) at a heating rate of 2 °C min<sup>-1</sup> to a given temperature for 1 h.

The FTS test used the syngas with a molar ratio of H<sub>2</sub>/CO = 2.0 and 3.0 MPa in pressure at a temperature specified. Before each FTS test, the mixed syngas composition was analyzed by an online GC and metered by a wet gas flow meter as tail gas. The online gas chromatograph (Model 7890B, Agilent, USA) is equipped with an HP-PONA column, a GS-GASPRO capillary column, an HP-PLOT 5A Molesieve porous layer open tubular column and an HP-PLOT-Q packed column to separate the tail gas mixture, which was then identified by one TCD and two FID detectors.

Each test lasted for over 100 hours. The water, oil and wax in the product were collected in a hot trap (150 °C) and a cold trap (0 °C) and analyzed by offline GCs. Carbon balances were calculated daily to ensure correct metering. For all the tests, the carbon balances were in the range of 97 – 101 %. To avoid large temperature fluctuation in the catalyst bed, the CO conversion was maintained within 10 – 20 % by setting different gas hourly space velocity (GHSV). The as-prepared and spent catalysts were taken out from the reactor under the protection of N<sub>2</sub> in a glove box and then sealed in FTS wax for characterization.

### 2.3 Characterization of MOFs and catalysts

A FEI Talos<sup>TM</sup> 200A microscope operated at 200 kV was employed to conduct structural investigations of various catalysts by using TEM, HRTEM, and STEM mode. The elemental maps were obtained by using high-angle annular dark-field scanning TEM (HAADF-STEM) of energy-dispersive X-ray (EDX) mode.

The X-ray diffraction pattern was recorded with an advanced D8 powder diffractometer (Bruker, Germany) using Co K $\alpha$  radiation ( $\lambda = 0.179$  nm) in the range of  $2\theta = 5 - 80$  °. The scan step was 0.02 °. The Co phase distribution is calculated by means of the Rietveld refinement. The average phase crystal size is calculated by Debye–Scherrer equation at the peak of 52.2 °.

Co K-edge X-ray absorption fine structure (XAFS) spectra were collected at beamline 1W1B of the Beijing Synchrotron Radiation Facility (BSRF), Institute of High Energy Physics (IHEP), Chinese Academy of Sciences. The typical storage ring energy was 2.5 GeV with a maximum current of 250 mA. The XAS spectra were taken repeatedly in the “transmission mode” from the wax-sealed samples. The Si (111) double crystal monochromator was used and detuned 35 % for Co in order to reduce the amount of higher harmonics in the beam. The photon energy was calibrated for each scan with the first inflexion point of the Co K edge (7709 eV) in Co metal foil. Fourier transform of the EXAFS spectra was carried out in the K-range of 3.0 to 12.8 Å<sup>-1</sup>. The IFFEFIT 1.2.11 data analysis package (Athena, Artemis, Atoms, and FEFF9.6) was used for the data analysis and fitting.

## 3 Results and discussions

Commercially, cobalt (Co) or iron (Fe)-based catalysts are used in the FTS process at 190 - 360 °C and 1.5 - 5.0 MPa.<sup>35</sup> The Co-based catalysts are normally used in the low-temperature range (190 - 240 °C), while the Fe-based catalysts can be extended to medium (260 - 300 °C) and high (320 - 360 °C) temperature ranges.

Cobalt is more active than iron in FTS. It has the advantage in limiting water-gas shift, yielding desired long-chain hydrocarbons ( $C_{5+}$ ) at temperatures below 240 °C, and resists to deactivation with a lifetime of over 10000 h.<sup>36-38</sup> At temperatures above 240 °C, cobalt catalysts do perform more actively but simultaneously promotes methanation resulting in much-lowered selectivity to the desired  $C_{5+}$ .<sup>39</sup> This causes the space-time yield of oil not more than 0.5 kg·kg-cat<sup>-1</sup>h<sup>-1</sup> in the existing industrial plants,<sup>40</sup> inhibiting the running of cobalt-catalyzed FTS at above 240 °C. Fabricating cobalt catalysts to have both high selectivity and activity at above 240 °C is hopeful to overcome this limitation.

In the initial stage of this work, we heated the Co-MOF in helium at 500 °C for 1 hour. The catalyst obtained (denoted as Co@C-500-He) showed the characteristic XRD patterns of the Co-MOF, cobalt oxide and metallic cobalt, suggesting only partial decomposition and reduction of the Co-MOF occurred in the pure Helium atmosphere (Figure S1, SI). The average crystal sizes calculated are 4.1 nm for the metallic phase. The catalyst was tested under the FTS reaction condition ( $H_2/CO = 2.0$ , 200 °C, 3.0 MPa). After the reaction, the  $Co^0$  crystal size dramatically increased to 18.8 nm. In contrast, a sample Co@C-500- $C_2H_2$  was prepared in the atmosphere of 2.0 %  $C_2H_2$  in Helium. Its XRD identified the  $Co^0$  phase mainly, suggesting a very high degree reduction of the Co-species. The  $Co^0$  crystal size is at 2.5 nm. After FTS tests, the  $Co^0$  crystal size increased to 5.0 nm. The preliminary studies verified that the  $C_2H_2$  plays a crucial role in facilitating reduction of the Co-MOF and the formation of smaller and more stable cobalt crystals as the high-performance FTS catalysts in a controllable manner (see more results in Table S1 and Figure S1, SI).

### 3.1 Core/shell Co@C nanoparticles prepared from Co-MOF

Ethyne starts a significant decomposition at the temperature of ~350°C (Figure S2, SI). The temperatures of 400, 450, 500, 550 and 600 °C were thus systematically applied for converting the Co-MOF to the core/shell Co@C catalysts in the presence of ethyne in He gas. The catalysts are denoted as Co@C-400, 450, 500, 550 and 600, respectively. The elemental and porosity analysis results in Table 1 show the samples increase their cobalt content and BET area. Both reach the maximum values as the temperature increases to 450 and 500 °C, respectively, above which these parameters decline. The trends reflect the carbon deposition amount increasing with temperature and the carbon deposited has the highest porosity at the temperature 500 °C and becomes denser after that.

**Table 1.** Properties of the Co MOF precursor and Co@C catalysts

Catalysts	Co content, %	BET Area, m <sup>2</sup> g <sup>-1</sup>	Surface elemental content <sup>a</sup> , %			$dp_{Co}$ , nm	
			Co	C	O	XRD <sup>b</sup>	TEM <sup>c</sup>
Co-MOF	14.6	107	7.1	66.3	26.6	-	
Co@C-400	24.6	41	11.5	67.6	20.9	-	3.2
Co@C-450	32.1	179	12.7	70.3	17.0	2.4	4.5
Co@C-500	31.7	337	9.0	78.4	12.6	2.5	2.8
Co@C-550	29.8	325	8.3	80.9	10.8	3.3	4.7
Co@C-600	28.1	271	6.6	87.4	6.0	3.7	6.2

<sup>a</sup> Analysed by XPS.

<sup>b</sup> Determined by XRD using Debye–Scherrer equation at the peak of 52.2 °.

<sup>c</sup> Determined from TEM by counting more than 200 particles.

The TEM/HRTEM analyses in Figure 1 clearly show the round-shaped  $\text{Co}^0$  nanoparticles encapsulated in carbon shells. The carbon shells in the  $\text{Co}@C-400$  and 450 are amorphous, while in the  $\text{Co}@C-500$ , -550 and -600 show layered-graphene sheets of 2 - 10 layers. Interestingly, the layer spacing is approximately 0.34 nm matching well with the graphite interplanar spacing (002) of 0.335 nm. Some graphene layers have dislocated, disordered or a combination of both lattice defects (Figure 1f and h),<sup>41</sup> which form the pores in the carbon shell. The  $\text{Co}^0$  nanoparticles appear in the size range of 2.0 - 10.0 nm (Figure 2). Statistically, the particle size distributions centre at 3.2, 4.5, 2.8, 4.7 and 6.2 nm for  $\text{Co}@C-400$ , -450, -500, -550, and -600, respectively.

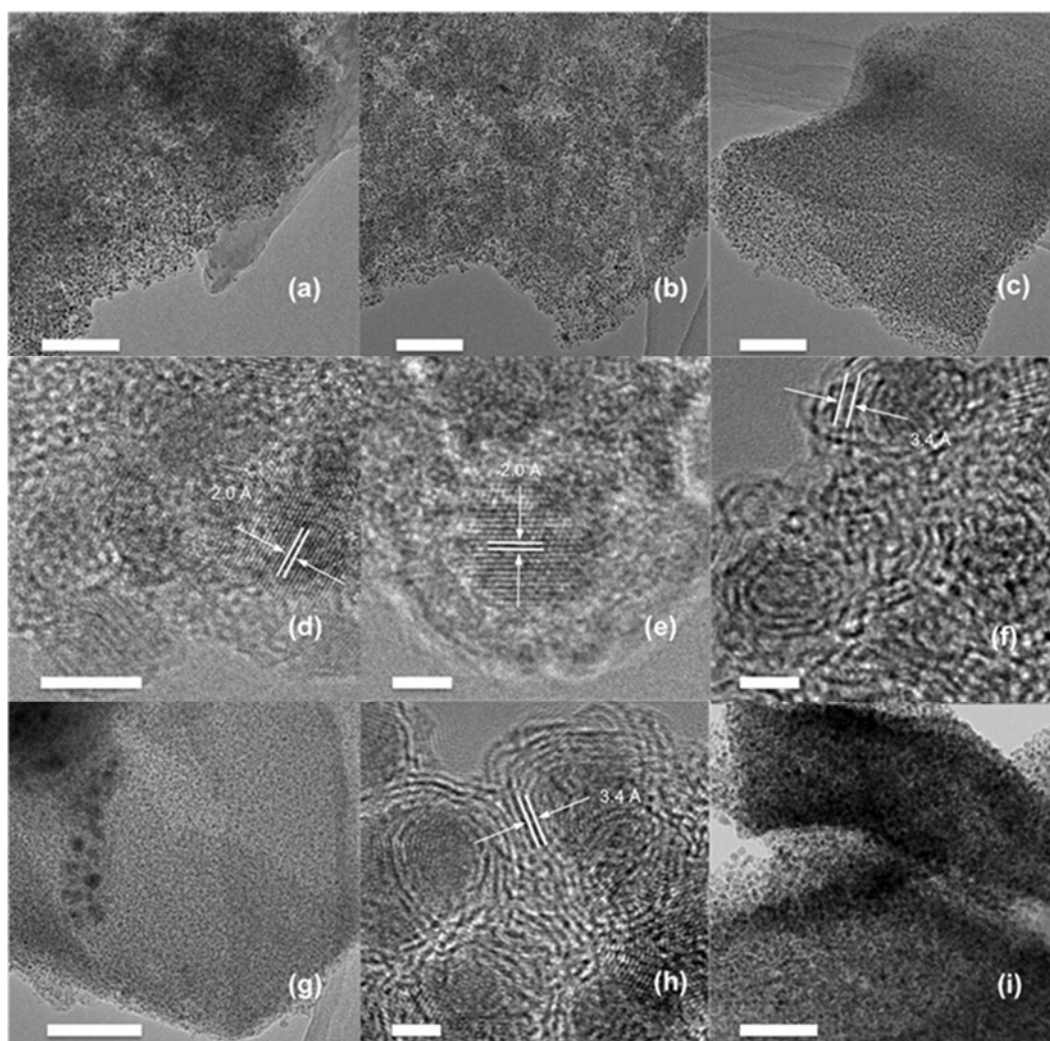


**Figure 1.** TEM images of the as-prepared  $\text{Co}@C-400$  (a, d), 450 (b, e), 500 (c, f), 550 (g, h), and 600 (i). Scale bar (a, b, c, g, i): 100 nm; (d): 5 nm; (e, f, h): 2 nm.

The XRD studies of these samples in Figure 3a show a significant fraction of Co-MOFs remained in the  $\text{Co}@C-400$  and a small fraction in the  $\text{Co}@C-450$ . At higher temperatures, the Co-MOF diffraction pattern disappeared completely. New wide and weak XRD peaks appear at  $2\theta = 43, 52$  and  $60^\circ$ , which are assignable to the CoO phase (JCPDS No.72-1474), face-centred-cubic (*fcc*)  $\text{Co}^0$  phase (JCPDS No.01-1259) and hexagonal-close-packed (*hcp*)  $\text{Co}^0$  phase (JCPDS No.01-1278), respectively. Calculation shows the  $\text{Co}@C-450$  contains 19.1 % CoO, 72.6 % *fcc* and 8.3 % *hcp*  $\text{Co}^0$ ; the  $\text{Co}@C-500$  5.0 % CoO, 88.5 % *fcc* and 4.0 % *hcp*  $\text{Co}^0$ ; while the  $\text{Co}@C-550$  and 600 catalysts contain the *fcc*  $\text{Co}^0$  phase only. Theoretically, the phase transformation of *hcp*  $\text{Co}^0$  to *fcc* occurs in the range of  $430 - 552^\circ\text{C}$ ,<sup>42,43</sup> the *fcc*  $\text{Co}^0$  is thermodynamically

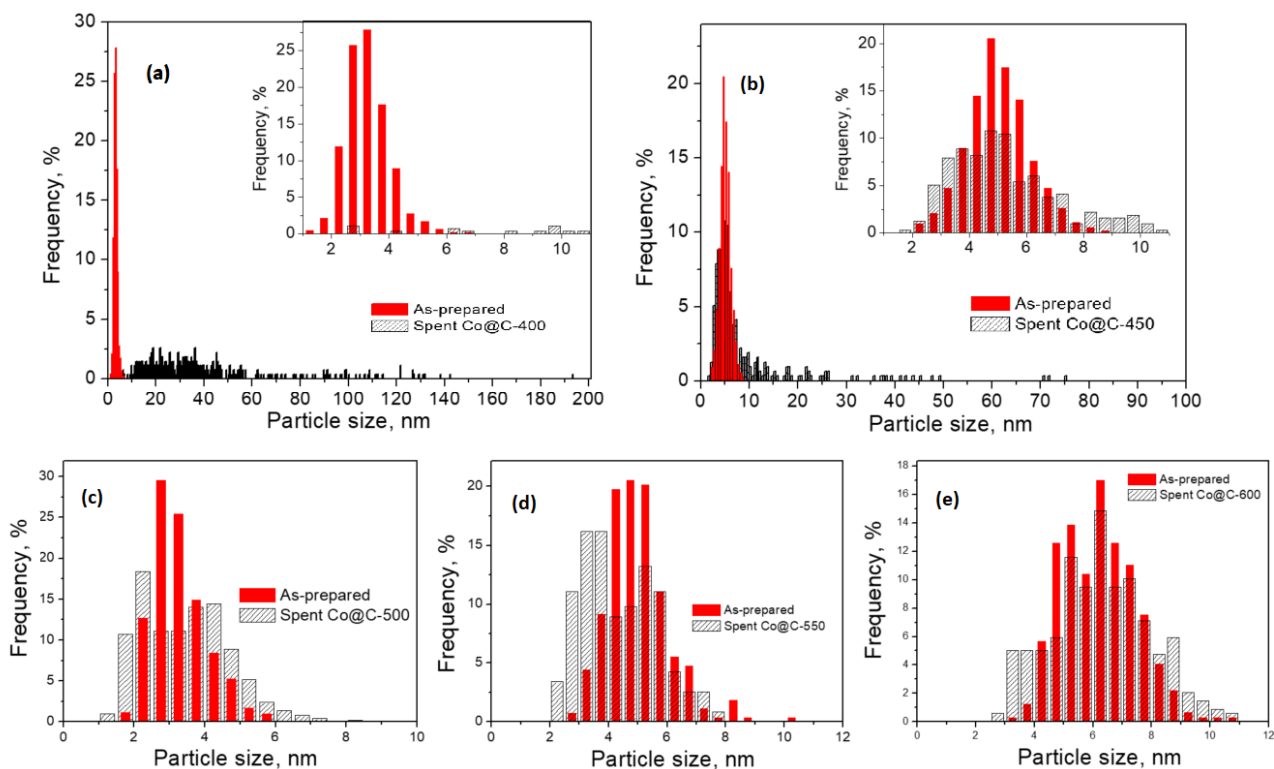


**Figure 2.** Size distributions of the Co nanoparticle in the as-prepared and spent catalysts: (a) Co@C-400; (b) Co@C-450; (c) Co@C-500; (d) Co@C-550 and (e) Co@C-600. The scale reflects the ranges detected.

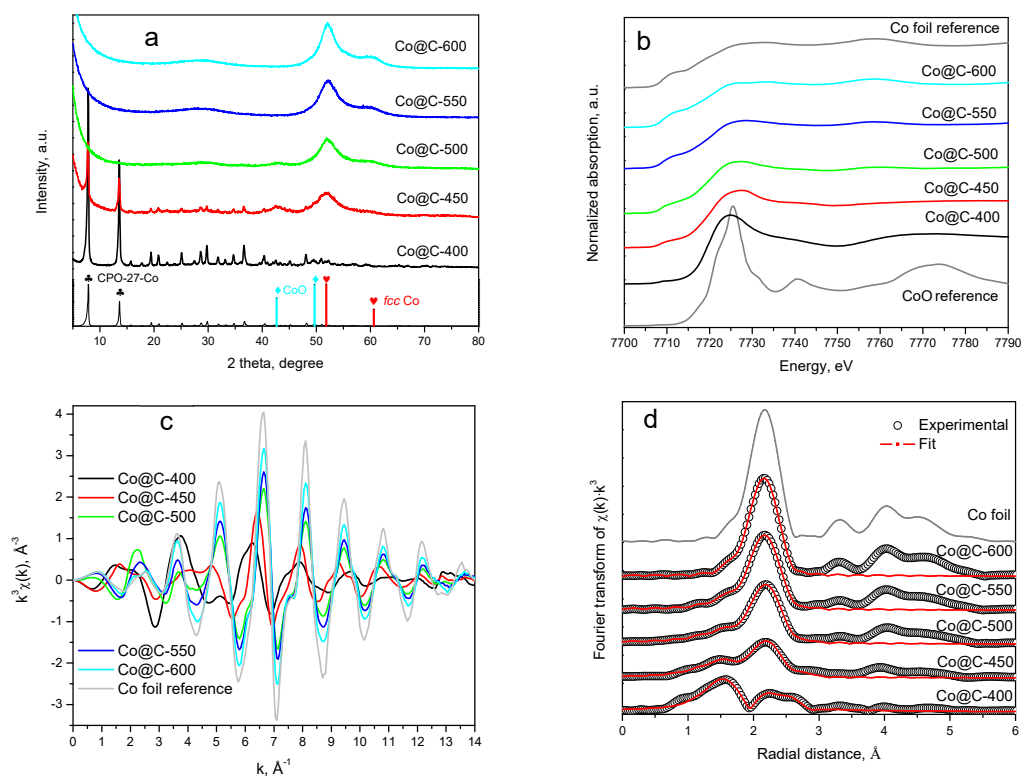


**Figure 3.** (a) XRD patterns; (b) Normalized Co K-edge XANES spectra; (c)  $k^3$ -weighted EXAFS  $\chi(k)$  function and (d) magnitude of the EXAFS Fourier transform of the Co@C catalysts as-prepared.

more stable than the *hcp* Co<sup>0</sup> at temperatures > 450 °C. Their coexistence has been found at temperatures up to 500 °C.<sup>44</sup> These explain the *fcc* Co<sup>0</sup> phase dominates in these samples. Both *hcp* and *fcc* phases are found in the Co@C-400. The *hcp* phase amount decreases with the treatment temperature and disappears at the temperatures > 500 °C e.g. the Co@C -550 and 600 contain purely *fcc* Co<sup>0</sup>. The Co<sup>0</sup> crystal size is observed in the range of 2.4 - 3.7 nm (see Table 1).

To detail the chemical states of cobalt in the Co@C catalysts, the X-ray absorption spectroscopy (XAS) has been applied with Co<sup>0</sup> foil and CoO as references. The Co *K*-edge X-ray absorption near edge spectra (XANES) are shown in Figure 3b. The position of *K* edge shifts towards a lower energy and the dramatic decrease of the white line intensity with the treatment temperatures show the reduction degree of the Co-MOF. As a direct measure of the density of empty states of the cobalt species at the Fermi level, the white line of the less reduced Co-MOF is stronger in intensity, while the fully reduced samples feature a very weak white line towards that of the Co<sup>0</sup> foil. This suggests a high reduction of -CoO- to Co<sup>0</sup> has been achieved in the Co@C-550 and 600, while the Co@C-400, -450 and -500 prepared at the lower temperatures contain Co in oxidized states. Quantitative analysis by a linear combination of the Co<sup>0</sup> foil and CoO spectra gives the Co<sup>0</sup> contents of 6.5, 54.7, 69.2, 87.8 and 94.1 % for the Co@C-400, 450, 500, 550 and 600, respectively.

More detailed Co coordination structures in the Co@C catalysts have been analyzed by Co *K*-edge *k*<sup>3</sup>-weighted extended X-ray absorption fine structure (EXAFS) spectra, as shown in Figure 3c. The EXAFS spectra of Co@C-500, -550 and -600 are very close to that of the Co<sup>0</sup> foil with slightly weaker oscillation, implying that the majority of cobalt species are metallic. The Co@C-400 and 450 feature stronger oscillation in the lower *k* range and a weak oscillation in the higher *k* range. As the EXAFS oscillation in the lower *k* range mainly comes from the electron scattering of relatively light atoms such as oxygen and carbon, whereas the oscillation in the higher *k* range is from the scattering of the heavy atoms such as cobalt here,<sup>45</sup> most of the Co atoms in Co@C-400 and -450 should be surrounded by oxygen and carbon atoms. In order to quantify the local environment of the Co atoms, the best-fits of the EXAFS scattering amplitudes were conducted through the Fourier transform. The results of the first two shells are shown in Figure 3d. The major peaks with the radial distance of 1.6 and 2.2 Å have been related to the -Co-O- and Co-Co interactions, respectively.

The spectrum of the Co@C-400 catalyst shows a strong peak for -Co-O- but a weak one for Co-Co, suggesting a small contribution from Co<sup>0</sup>. As the C<sub>2</sub>H<sub>2</sub> treatment temperature increases, a large fraction of the cobalt becomes Co<sup>0</sup> and the Co-Co peak becomes prominent. The EXAFS spectrum of the Co@C-600 appears virtually identical to that of the Co<sup>0</sup> foil. All the Co@C catalysts feature a Co-Co shell with a Co-Co distance of 2.47 - 2.50 Å and a coordination number ranging from 3.0 to 10.0. The number of Co neighbouring atoms in the shell is related to the reduction degree and the Co<sup>0</sup> particle size in catalysts.<sup>46</sup> Apparently, increasing C<sub>2</sub>H<sub>2</sub> treatment temperature will lead to an increase of Co-Co coordination number *N*<sub>Co-Co</sub>. A value of 10.0 is achieved in the Co@C-600, slightly smaller than 12.0 for the closest packed structure of bulk Co<sup>0</sup>. The EXAFS results of the catalysts as-prepared and the spent are summarized in Table 2.

**Table 2.** EXAFS results at the Co K-Edge for the Co@C catalysts as-prepared and after FTS reaction

Catalysts	States	Co <sup>0</sup> , % <sup>a</sup>	N <sub>Co-O</sub> in CoO	R <sub>Co-O</sub> in CoO, Å	σ <sup>2</sup> , Å <sup>2</sup>	N <sub>Co-Co</sub> in Co <sup>0</sup>	R <sub>Co-Co</sub> in Co <sup>0</sup> , Å	σ <sup>2</sup> , Å <sup>2</sup>
Co@C-400	As-prepared	6.5	6.1	2.12	0.012	3.1	2.50	0.012
	Spent	7.8	5.6	2.12	0.017	4.9	2.49	0.008
Co@C-450	As-prepared	54.7	4.8	2.11	0.010	3.0	2.48	0.006
	Spent	58.8	4.2	2.10	0.018	6.4	2.47	0.007
Co@C-500	As-prepared	69.2	4.4	2.11	0.015	6.1	2.48	0.007
	Spent	69.8	4.1	2.11	0.014	6.0	2.48	0.007
Co@C-550	As-prepared	87.8	1.2	2.11	0.007	7.8	2.48	0.007
	Spent	69.4	3.6	2.12	0.009	6.1	2.49	0.006
Co@C-600	As-prepared	94.1	0.5	2.11	0.008	10.0	2.48	0.007
	Spent	73.1	1.9	2.11	0.010	7.9	2.49	0.007

<sup>a</sup> Extent of Co reduction calculated by a linear combination of the XANES spectra of Co foil and CoO references.

The size of Co<sup>0</sup> nanoparticles is determined by the formation of the carbon shell. The formation of the Co<sup>0</sup> nanoparticles includes the Co-species reduction, nucleation and crystal growth steps, which is significantly impacted by the reducing atmosphere, reaction temperature and time. Whereas, the carbon shell builds up a physical barrier on the Co<sup>0</sup> nanoparticles to hinder cobalt particle further growing. The forming rates of Co<sup>0</sup> nanoparticles and carbon shells control the size of the Co<sup>0</sup> nanoparticles encapsulated and the size distribution. From our observation, the C<sub>2</sub>H<sub>2</sub> treatment at 500 °C would provide an optimal condition for facilitating the formation of the smallest Co@C nanoparticles of 2.8 nm in average with a narrowest size distribution. Of course, under the C<sub>2</sub>H<sub>2</sub> chemical vapour deposition condition the structure and size of the Co<sup>0</sup> cores and the carbon shells composed of either amorphous carbon or graphene become more controllable.

### 3.2 FT catalysis of the core/shell cobalt nanoparticles

The activity and selectivity of FTS catalysis are closely related to the reaction conditions, in particular the temperature. The Co@C-500 was chosen to examine the catalysis performance of the Co@C in a wide temperature range from 150 to 320 °C. The catalysts were on stream tested at a given temperature for over 100 hours. The results are given in Table 3 and Figure 4. As well as the actual CO conversion (X<sub>CO</sub>, %) measured, the CTY and TOF (turnover frequency) are provided for examining the catalytic activity. The TOF is defined as the moles of CO converted per mole of surface cobalt per second, and CTY is defined as the moles of CO converted to hydrocarbons per gram of cobalt per second. The CO<sub>2</sub> selectivity (S<sub>CO2</sub> %) and hydrocarbon distribution are applied in order to show the catalytic selectivity.

At the temperature of as low as 150 °C, the Co@C-500 shows a significant TOF value at 0.9 x 10<sup>-3</sup> s<sup>-1</sup>, which steadily increases to 3.9 x 10<sup>-3</sup> s<sup>-1</sup> at 180 °C, 21.6 x 10<sup>-3</sup> s<sup>-1</sup> at 220 °C, 57.7 x 10<sup>-3</sup> s<sup>-1</sup> at 280 °C and 64.6 x 10<sup>-3</sup> s<sup>-1</sup> at 320 °C. These TOF values are compared with those in literature as shown in Figure 4a.<sup>18,24,47-52</sup> It can be seen that the TOFs vary in a wide range in the popularly studied temperature range of 200 - 220 °C. The variation is to do with the cobalt nanoparticle sizes, support materials and reaction conditions. In the well-validated references at the similar reaction conditions, the cobalt particles with a size of 2.5 nm on carbon

**Table 3.** The catalytic performances of the Co@C catalysts in FTS reactions <sup>a</sup>

Catalysts	T, °C	GHSV, h <sup>-1</sup>	X <sub>CO</sub> , %	CTY <sup>b</sup>	TOF <sup>c</sup>	CO <sub>2</sub> , %	S <sub>c</sub> , %			O/P	α
							CH <sub>4</sub>	C <sub>2-4</sub>	C <sub>5</sub> <sup>+</sup>		
Co@C-500 <sup>d</sup>	150	2000	7.3	4.5	0.9	0.0	2.4	1.9	95.7	0.78	0.95
	180	2000	33.3	20.6	3.9	0.0	4.6	4.4	91.0	0.64	0.92
	200	10000	21.6	66.3	12.6	0.8	6.4	6.1	87.5	0.56	0.90
	220	20000	18.4	111.5	21.6	2.1	8.2	7.5	84.3	0.49	0.89
	240	40000	15.7	187.9	36.8	3.5	9.9	8.7	81.4	0.35	0.87
	260	60000	13.7	242.3	48.2	4.8	13.0	11.6	75.4	0.26	0.84
	280	60000	15.6	286.1	57.7	6.1	18.7	18.4	62.9	0.21	0.80
	300	60000	17.2	290.2	60.3	8.9	27.4	33.2	39.4	0.06	0.66
	320	60000	18.4	294.2	64.6	13.8	41.8	49.5	8.6	0.01	0.40
Co@C-400 <sup>e</sup>	260	8000	12.6	44.5	-	6.9	27.4	20.3	52.3	0.40	0.76
Co@C-450 <sup>e</sup>	260	60000	18.6	312.1	76.8	6.5	21.9	19.7	58.4	0.33	0.78
Co@C-500 <sup>e</sup>	260	60000	14.4	254.1	50.5	4.7	13.3	11.6	75.1	0.26	0.85
Co@C-550 <sup>e</sup>	260	50000	16.8	186.0	38.4	4.7	11.7	10.7	77.6	0.27	0.87
Co@C-600 <sup>e</sup>	260	20000	13.2	89.7	19.4	4.9	10.3	7.7	82.0	0.28	0.89

<sup>a</sup> Reaction condition: 150 - 320 °C, H<sub>2</sub>/CO = 2.0, 3.0 MPa, GHSV = 2000 - 60000 h<sup>-1</sup>.

<sup>b</sup> CTY = 10<sup>-6</sup> mol g<sub>Co</sub><sup>-1</sup> s<sup>-1</sup> based on mole of CO converted to hydrocarbons per gram of cobalt per second.

<sup>c</sup> TOF = 10<sup>-3</sup> s<sup>-1</sup> based on mole of CO converted per mole of surface cobalt per second.

<sup>d</sup> Results of the conditional FTS runs at varied temperatures.

<sup>e</sup> The long-time steady-state test results of the Co@C-400-600 catalysts.

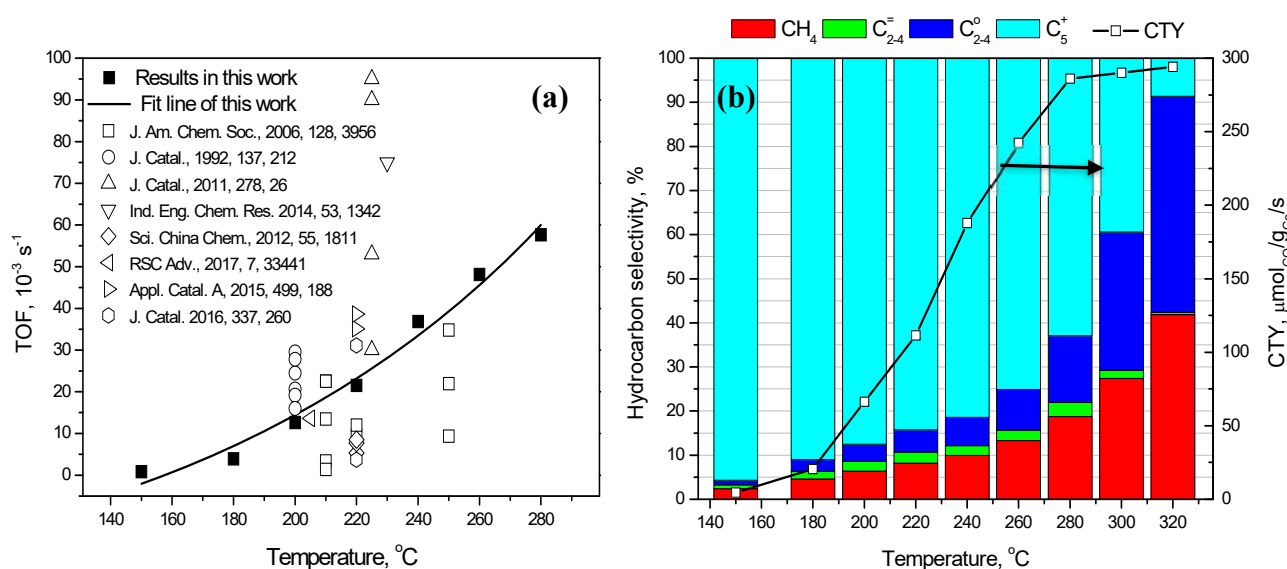


**Figure 4.** The FTS catalytic activity and selectivity of the Co@C-500 at different reaction temperatures: (a) TOF; (b) CTY and hydrocarbon distribution. (P = 3.0 MPa, GHSV= 2000 - 60000 h<sup>-1</sup>)

nanofibers were found having a TOF levelled at  $1.4 \times 10^{-3} \text{ s}^{-1}$  at  $210 \text{ }^\circ\text{C}$  and  $3.5 \text{ MPa}$ .<sup>18</sup> Over carbon nanotube or carbon sphere supported cobalt particles with a size of  $3.0 \text{ nm}$ , the TOF was found to be ca.  $30 \times 10^{-3} \text{ s}^{-1}$  at  $225 \text{ }^\circ\text{C}$  and  $0.8 \text{ MPa}$ .<sup>40</sup> In our work, the TOF value from the  $\text{Co}^0$  nanoparticles of  $3.0 \text{ nm}$  is  $21.6 \times 10^{-3} \text{ s}^{-1}$  at  $220 \text{ }^\circ\text{C}$  and  $3.0 \text{ MPa}$ , which is at a similar level to that of the cobalt nanoparticles on carbon nanotube or carbon sphere<sup>40</sup> and distinctively higher than those on carbon nanofiber.<sup>18</sup>

At  $150 \text{ }^\circ\text{C}$ , the CTY was low at  $4.5 \times 10^{-6} \text{ mol g}_{\text{Co}}^{-1}\text{s}^{-1}$ . When the temperature raised from  $180$  to  $280 \text{ }^\circ\text{C}$ , the CTY increased exponentially as expected from  $20.6 \times 10^{-6}$  to  $286.1 \times 10^{-6} \text{ mol g}_{\text{Co}}^{-1}\text{s}^{-1}$ . The CTY value reads  $88.9 \times 10^{-6}$  at  $210 \text{ }^\circ\text{C}$  and  $215 \times 10^{-6} \text{ mol g}_{\text{Co}}^{-1}\text{s}^{-1}$  at  $250 \text{ }^\circ\text{C}$ , which are indeed higher than the  $43.5 \text{ } \mu\text{mol}_{\text{CO}} \cdot \text{g}_{\text{Co}}^{-1} \cdot \text{s}^{-1}$  (at  $210 \text{ }^\circ\text{C}$ ,  $3.5 \text{ MPa}$ ) and  $192.0 \text{ } \mu\text{mol}_{\text{CO}} \cdot \text{g}_{\text{Co}}^{-1} \cdot \text{s}^{-1}$  (at  $250 \text{ }^\circ\text{C}$ ,  $3.5 \text{ MPa}$ ) optimised for the  $6 - 8 \text{ nm}$   $\text{Co}^0$  nanoparticles on carbon nanofibers.<sup>18</sup> Moreover, the selectivity to  $\text{C}_{5+}$  at  $150 \text{ }^\circ\text{C}$  is greater than  $95 \%$  with a growth probability  $\alpha$  value of  $0.95$  and a negligible  $\text{CO}_2$  yield. When the temperature was raised from  $180$  to  $280 \text{ }^\circ\text{C}$ , the  $\text{C}_{5+}$  fraction decreased gradually to  $62.9 \%$  and  $\text{CO}_2$  gas yield increased to  $6.1 \%$ . Above  $280 \text{ }^\circ\text{C}$ , the CTY increase was dramatically reduced and the product dominated by the light hydrocarbons ( $\text{C}_{1-4}$ ), which is not desirable for liquid hydrocarbon production. The corresponding  $\alpha$  values gradually decreased to  $0.85$  at  $260 \text{ }^\circ\text{C}$  and  $0.40$  at  $320 \text{ }^\circ\text{C}$ . An example of Anderson-Schultz-Flory distribution of hydrocarbon products can be found in SI (Figure S15).

The  $\text{Co}@C-500$  demonstrates high catalytic activity at a medium temperature of  $260 \text{ }^\circ\text{C}$ , which is accompanied by a good selectivity to  $\text{C}_{5+}$  of  $75 \%$ , low conversion to  $\text{CO}_2$  at  $4.8 \%$ . These are outstanding results in the literature and obviously better than that from the MOF-derived catalyst produced by simple pyrolysis in inert gas.<sup>10</sup> The latter contained  $\text{Co}^0$  nanoparticles of  $10 - 12 \text{ nm}$  in carbon matrix and gave a selectivity to  $\text{C}_{5+}$  at  $65 \%$  and  $\text{CO}_2$  selectivity at  $8.0 \%$  at  $230 \text{ }^\circ\text{C}$ .<sup>10</sup> Taking both the CTY and  $\text{C}_{5+}$  selectivity into consideration, the temperature of  $260 \text{ }^\circ\text{C}$  was selected to test this series of catalysts, which is in the medium temperature range for FTS and not normally recommended for cobalt-based catalysts.<sup>35</sup> Development of cobalt catalysts feasible to operate at  $260 \text{ }^\circ\text{C}$  will be beneficial for generating a higher quality of steams from the exothermic reactions ( $\Delta H = 165 \text{ kJ mol}^{-1}$ ) and improving the process energy efficiency.

The series of  $\text{Co}@C-400$  to  $600$  catalysts were then prepared on stream and tested at  $260 \text{ }^\circ\text{C}$  for over  $100$  hours. The results are given in Table 3. In general, this series of catalysts exhibit excellent activity and stability. Very impressive specific activity CTY at  $254.1 - 312.1 \text{ } \mu\text{mol}_{\text{CO}} \cdot \text{g}_{\text{Co}}^{-1} \cdot \text{s}^{-1}$  was achieved using the  $\text{Co}@C-450$  and  $-500$  at GHSV  $60000 \text{ h}^{-1}$ . The  $\text{Co}@C-500$  showed a higher selectivity to  $\text{C}_{5+}$  ( $> 75 \%$ ) than  $\text{Co}@C-450$  ( $58.4 \%$ ). For the  $\text{Co}@C-550$  and  $600$ , the GHSVs were reduced to  $50000$  and  $20000 \text{ h}^{-1}$ , respectively, in order to maintain the CO conversion at a comparable level ( $10 - 20 \%$ ). Their CTY values decreased to  $186.0$  and  $89.7 \text{ } \mu\text{mol}_{\text{CO}} \cdot \text{g}_{\text{Co}}^{-1} \cdot \text{s}^{-1}$ , respectively. This displays their relatively lower activities under the FTS conditions used. Even so, their  $\text{C}_{5+}$  selectivities are at  $77.6 \%$  and  $82.0 \%$ , which is better than that of the  $\text{Co}@C-500$ . The  $\text{Co}@C-400$  required a much longer residence time (GHSV =  $8000 \text{ h}^{-1}$ ) than the other catalysts for a CO conversion of  $10 - 20 \%$ , possessed the lowest activity (CTY =  $44.5 \text{ } \mu\text{mol}_{\text{CO}} \cdot \text{g}_{\text{Co}}^{-1} \cdot \text{s}^{-1}$ ) and  $\text{C}_{5+}$  selectivity ( $52.3 \%$ ). The good activity demonstrated by the catalyst  $\text{Co}@C-450$  and  $500$  give rise to high hydrocarbon and  $\text{C}_{5+}$  space-time yields of  $4.0 - 5.2 \text{ g}_{\text{HC}} \cdot \text{g}\text{-cat}^{-1} \cdot \text{h}^{-1}$  and  $3.03 \text{ g}\text{-g-cat}^{-1} \cdot \text{h}^{-1}$ , respectively. The higher  $\text{C}_{5+}$

selectivity and  $\alpha$  values on the Co@C-500 to 600 catalysts reveal the direct relationship of their unique Co@C structures to long-chain hydrocarbon formation. This will be further discussed in the following sections.

### 3.3 Effect of catalyst structure on the FT catalysis

The spent catalysts were examined by TEM and HRTEM for their changes in structure and morphology. Similar to the as-prepared samples, all the spent catalysts contain Co<sup>0</sup> nanoparticles, as exemplified in Figure 5 and Figure S3-4 (SI). For verifying the effect of the carbon structure, the spent Co@C catalysts were treated with a 0.5 M aqueous solution of hydrochloric acid, followed by washing using deionized water and toluene to remove all the cobalt species and wax. After the Co<sup>0</sup> crystallites eroded away, the solid residual shows amorphous carbon with little regular graphene structures from the spent Co@C-400 and 450 catalysts (Figure 5c; Figure S5-6, SI), but curly and wrinkled graphene sheets with obvious bubble cavities from the spent Co@C-500, 550 and 600 (Figure 5f; Figure S7-9, SI). The latter have cavities in the size range of approximately 3.0 – 10.0 nm, well matching the Co<sup>0</sup> nanoparticle sizes in these samples (Figure 2c-e). This infers that the carbon shells play the role well in protecting the nanoparticles from aggregations during the FTS reaction. The successful removal of Co<sup>0</sup> cores suggests that the graphene shells are porous, providing pathways to control the diffusion of reactants through the carbon shell to the active surface of Co<sup>0</sup> core for the reaction and the release of products.

More interestingly, the Co<sup>0</sup> nanoparticles can be removed from the spent Co@C-400 to -550 samples by an overnight acid-leaching, while the spent Co@C-600 needs a much longer time (e.g. one week) to reach a complete removal. This result agrees well with the BET area changes as shown in Table 1, suggesting that the Co<sup>0</sup> nanoparticles in Co@C-600 are encapsulated by low porosity of carbon, are less accessible due to a higher degree of graphitization of the carbon shell. More than 10 graphite layers are observed from the TEM images (Figure S9, SI). The well-graphitized carbon shells could impede the access of syngas to the Co<sup>0</sup> cores, resulting in the Co@C less or inactive to the FTS catalysis.<sup>12, 51</sup> Controlling formation of porous carbon shells is critical for opening the active sites to the reactants. At a temperature lower than 600 °C, the ethyne deposition facilitates the formation of porous carbon shells varying from amorphous to graphene with different degrees of graphitization. The resulted structure distinctly differs from the metal@carbon-onions where the graphitized carbon materials are in focus.<sup>23-28</sup> The defects formed in graphitization create transport channels to the active metal nanoparticles encapsulated. The higher the C<sub>2</sub>H<sub>2</sub> treatment temperature, the higher the resistance of the carbon shell to the acid leaching. At the temperature of 500 °C, the curly and wrinkled graphene sheets formed provide transport channels with less resistance than that at 600 °C, allowing a more effective diffusion for both the reactant and the product. This trend agrees well with the pyrolysis results of ZIF-67, where the nitrogen-carbon composite shells of Co<sup>0</sup> nanoparticles formed at 600 - 900 °C was reported much difficult to penetrate.<sup>13</sup>

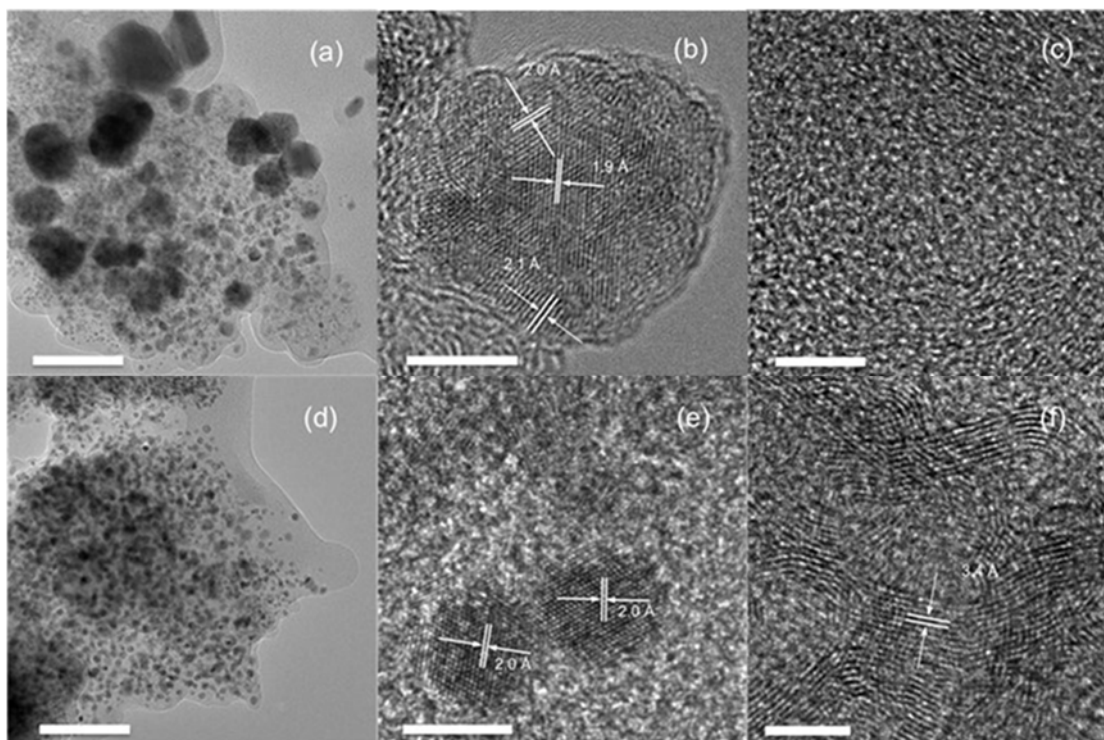


**Figure 5.** The TEM images of spent catalysts (a, b: Co@C-450; d, e: Co@C-500) and their carbon residues after acid pickling (c: Co@C-450; f: Co@C-500). Scale bar a, d: 100 nm; b, c, e, f: 5 nm.

Statistical size analysis (Figure 2) shows that the amorphous carbon encapsulated samples of the Co@C-400 and -450 has much larger Co<sup>0</sup> nanoparticles over 10 - 100 nm (Figure 2a and b), while the graphene sheet encapsulated samples largely maintained their respective particle size distributions as the as-prepared samples (Figure 2c, d and e). The size increases in the spent Co@C-400 and -450 could result from the crystal aggregation, but more likely from the crystal growth with the Co-MOF being further reduced. The reduction results in the metallic Co<sup>0</sup> fraction increase, as quantitatively calculated from the XANES given in Figure S10 (SI) and Table 2. Comparing the spent sample with the as-prepared, the Co<sup>0</sup> fraction increases from 6.5 to 7.8 % in Co@C-400 and 54.7 to 58.8 % in Co@C-450. Furthermore, the XRD analysis reveals the *fcc* and *hcp* Co<sup>0</sup> constituents changed as well. 63.8 % *fcc* and 36.2 % *hcp* are in the spent Co@C-400; 71.3 % *fcc* and 28.7 % *hcp* in the spent Co@C-450. Compared with the as prepared the *hcp* phase underwent a dramatic increase after the FTS reactions e.g. from non-detectable to 36.2 % in Co@C-400 and from 10.3 to 28.7% in Co@C-450, while the *fcc* phase remained relatively stable. These two catalysts containing more *hcp* Co<sup>0</sup> phase showed significantly higher site activities (TOF values of 76.8 and 50.5 × 10<sup>-3</sup> s<sup>-1</sup>) than the catalysts with less or no *hcp*-Co<sup>0</sup> phase, namely 8.4 % *hcp* in the spent Co@C-500 and no *hcp* in the spent Co@C-550 and -600. These results agree well with those in the literature, showing that *hcp*-Co<sup>0</sup> is probably more active than *fcc*-Co<sup>0</sup>.<sup>16,52-56</sup> The *hcp*-Co<sup>0</sup> phase was also found more selective to C<sub>5+</sub> in literature.<sup>57</sup> In this research, however, the *fcc*-Co<sup>0</sup> phase dominated catalysts Co@C-500 ~ 600 are more selective to C<sub>5+</sub>. The graphene layers on the Co nanoparticles may contribute to this, like that the carbon nanotubes (CNT) do to iron catalysts as reported by Chen et al,<sup>58,59</sup> but in this case the encapsulation of porous graphene shell could make more contribution to the high hydrocarbon selectivity.

The XANES spectra give the metallic  $\text{Co}^0$  of 69.8, 69.4, and 73.1 % in the spent  $\text{Co}@C-500$ , -550 and -600 (Table 2), respectively. Compared with the 69.2, 87.8 and 94.1 % in the as-prepared catalysts, the  $\text{Co}^0$  proportion change in the spent  $\text{Co}@C-500$  at 0.6 % is ignorable. The  $\text{Co}^0$  proportions in the spent  $\text{Co}@C-550$  and 600 dramatically declined by 18.4 and 21.0 %, respectively. Interestingly, their corresponding CTY values at the end of the reaction drastically increased (Table 3). This infers that the  $\text{Co}^0$  concentration is not the only factor influencing the catalyst activity. Although the cobalt metallic phases supply active sites for the FTS reactions, as shown in this research and in the literature, the complex nature of these active sites has not been fully understood yet. Conventional cobalt catalysts are usually formulated with supporters such as  $\text{TiO}_2$ ,  $\text{SiO}_2$  or  $\text{Al}_2\text{O}_3$  and promoters, leading to complex chemical environments for the Co species, exactly defining the active sites becomes very difficult. Compared with the other catalysts, the  $\text{Co}@C$  catalysts are much simpler in composition, for example, the catalyst  $\text{Co}@C-500$  contains 69.8 %  $\text{Co}^0$  and 30.2 %  $-\text{CoO}-$  in clearly-defined graphene shells only.

The EXAFS oscillation analysis results of the spent catalysts in Table 2 show very interesting variation in the coordination numbers of the Co-Co ( $N_{\text{Co-Co}}$ ) and Co-O ( $N_{\text{Co-O}}$ ) shells. The well-performed catalysts have  $N_{\text{Co-Co}} = \sim 6.0$  and  $N_{\text{Co-O}} = \sim 4.0$  in their spent forms. Thus, three types of changes have been found in the  $N_{\text{Co-Co}}$  and  $N_{\text{Co-O}}$  during the FTS process. On the average, in  $\text{Co}@C-400$  and -450, the  $N_{\text{Co-Co}}$  increases from 3.0 to 5.7 and the  $N_{\text{Co-O}}$  decreases from 5.5 to 4.9; while in  $\text{Co}@C-550$  and -600, the  $N_{\text{Co-Co}}$  decreases from 9.0 to 7.0 and the  $N_{\text{Co-O}}$  increases from 0.9 to 2.8. Finally, in  $\text{Co}@C-500$ , both the  $N_{\text{Co-Co}}$  and the  $N_{\text{Co-O}}$  are basically maintained without considerable changes. These trends associate well with their individual catalysis profiles (Figure 6). That is, the activities continuously decrease in  $\text{Co}@C-400$  and 450, increases in  $\text{Co}@C-550$  and -600, and remains stable in  $\text{Co}@C-500$ . This may suggest that the Co-Co and Co-O complexes exist on the surface of  $\text{Co}^0$  nanoparticles and reach an equilibrium state under the experimental conditions, where the  $N_{\text{Co-Co}}$  and  $N_{\text{Co-O}}$  are kept at  $\sim 6.0$  and  $\sim 4.0$ , respectively. This observation is supported by the findings in the references 17 and 18.

Two types of surface reactions might have occurred. For the catalyst  $\text{Co}@C-550$  and -600, the oxidation from the CO dissociation over the  $\text{Co}^0$  nanoparticles results in  $N_{\text{Co-O}}$  increasing and  $N_{\text{Co-Co}}$  decreasing. These two coordination numbers tend to achieve  $\sim 4.0$  and  $\sim 6.0$  through adjusting the Co-Co and Co-O configuration in the catalyst. This may explain the induction periods for the  $\text{Co}@C-550$  and -600 as observed in Figure 6. For the  $\text{Co}@C-400$  and -450, the hydrogen in the syngas plays a role in gradually reducing Co-O nanoclusters in MOFs or the Co-O structures on the catalyst surface, thereby the  $N_{\text{Co-O}}$  is decreased and the  $N_{\text{Co-Co}}$  is increased. This interpretation seems rational when considering the Co coordination number 5.0 – 6.0 in the Co-MOF. The latter mechanism has been approved by the *in-situ* XRD analysis of the Co-MOF stability test in 5.0 %  $\text{H}_2$  in Helium at 220 °C (Figure S11,SI), in which the reduction of Co-MOFs to form  $\text{Co}^0$  nanoparticles has been initially observed. In the CO gas, the Co-MOFs behave quite stable without decomposition. This justification is in line with very recent findings in the literature from *in-situ* XANES and XPS characterisation that the existing cobalt oxide may help facilitating the FTS reaction more than the fully reduced cobalt when supported on  $\text{TiO}_2$ .<sup>60</sup>

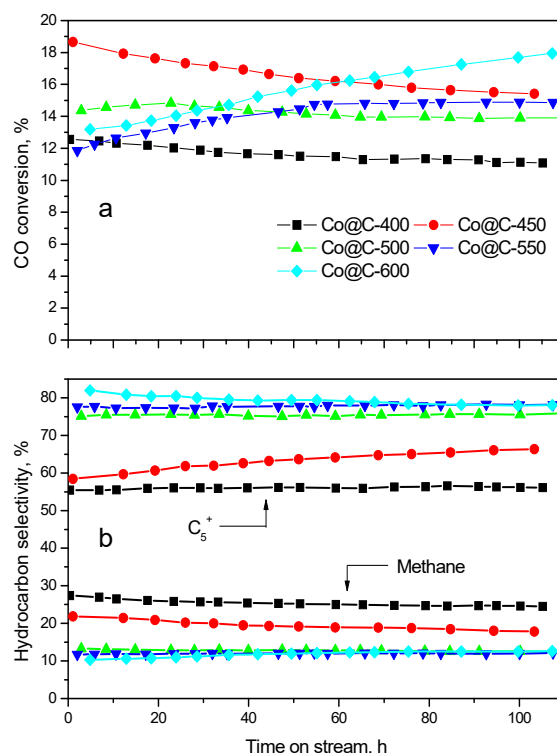


**Figure 6.** Variation of (a) CO conversion and (b) hydrocarbon selectivity of the Co@C-400 ~ -600 catalysts with FTS reaction time. Reaction conditions: 260 °C, 3.0 MPa, H<sub>2</sub>/CO = 2 (v/v) and GHSV of 8000 – 60000 h<sup>-1</sup>.

The most effective catalysts Co@C-450 and -500 in the current work have the Co<sup>0</sup> nanoparticles averaged at approximately 2.5 nm, which is obviously smaller than the critical sizes as reported in the literature.<sup>18,22-25</sup> This shift does not cause a decrease in the catalytic activity. In contrast, the small Co<sup>0</sup> nanoparticles with a Co-O phase existing on the surface demonstrated high catalytic activity. The high CTY values obtained are virtually constant throughout the FTS test. From the catalysis results and the catalyst structures, we derive that the composition of Co-Co and Co-O on the Co<sup>0</sup> nanoparticle surface and the pore structure of the carbon shell can promote the activity and selectivity, even at the medium temperature. Although the lower activity of the Co@C-550 and -600 catalysts results from the less permeable highly-graphitised carbon shells, these carbon shells afford the catalysts the higher selectivity of C<sub>5</sub><sup>+</sup>. This case is like that the iron active sites encapsulated in carbon nanotube (CNT) has a higher C<sub>5</sub><sup>+</sup> selectivity than that sit on the outside of CNTs or activated carbons.<sup>58,59</sup> Both the literature and our findings reported herein suggest that the core/shell Co@C nanoparticles fabricated from Co-MOF through ethyne reduction are highly active and selective in FTS catalysis at a medium temperature. The presence of porous carbon shell and -Co-O- phase on the surface of Co<sup>0</sup> nanoparticles might improve CO dissociation and chain propagation. It is clear that the carbon shell structure effectively contributes to the selectivity and activity of the Co@C catalysts. It will be interesting to understand more about the function of porous carbon shell and the effect of surface Co-O structures.

## 4 Conclusion

In this research, a new reducing MOF approach has been established to control the fabrication of core/shell Co@C nanoparticles by chemical vapour deposition of ethyne. The derived Co@C particles have been tested as FTS catalysts. The C<sub>2</sub>H<sub>2</sub> deposition over the Co-MOF effectively controlled the reduction of Co-O nanoclusters in the MOF frameworks into Co<sup>0</sup> nanoparticles. The hydrogen liberated from the C<sub>2</sub>H<sub>2</sub> decomposition acts as the reductant agent, and the rejected carbon encapsulates Co<sup>0</sup> nanoparticles and effectively restricted the freshly formed nanoparticles from aggregation. The treatment temperature controls the cobalt nanoparticle formation rate, crystal phase ratio, particle size, as well as carbon deposition rate and structures. At a deposition temperature below 450 °C, the carbon shell is amorphous. Above 500 °C, the porous graphene sheets are formed. The phase transition from the *hcp* to the *fcc* phase completes. The porous graphene shell not only plays the role in keeping the Co particles small at ~ 3.0 nm but also promotes the catalysis effectively at a medium temperature to produce long-chain hydrocarbons, which differs from other Co@Cs with non-porous graphitic carbon shells. The Co nanoparticles containing both the *fcc* and *hcp* phases showed high CTY values at ~ 254.1 - 312.1 μmol<sub>CO</sub>·g<sub>Co</sub><sup>-1</sup>·s<sup>-1</sup>, high hydrocarbon space-time yield of 4.0 - 5.2 kg<sub>HC</sub>·kg<sub>cat</sub><sup>-1</sup>·h<sup>-1</sup> and selectivity of ~ 70 - 80 % to the C<sub>5+</sub> fraction. The XANES and EXAFS spectra analyses identify the composition of the Co nanoparticles, the coordination numbers of Co-Co in the metallic core and -Co-O- on the Co<sup>0</sup> nanoparticle surface. The comprehensive evaluation of Co@C catalysts with respect to their performance in the FTS reaction implies that the Co-Co and Co-O coordination numbers of the Cobalt nanoparticles have considerable impact on the activity of the cobalt catalysts, while the porosity of the carbon shell mainly on the selectivity toward C<sub>5+</sub> production.

### ASSOCIATED CONTENT

Supporting Information

XRD, TGA, TEM, XPS and Fischer-Tropsch products.

### AUTHOR INFORMATION

Author Contributions

X. Guo and C. Zhang performed the most experiments and data analysis. They contributed equally.

Corresponding Author

\*zhangchh@sxicc.ac.cn; q.yuan@aston.ac.uk; b.xiao@qub.ac.uk; ywl@sxicc.ac.cn

Note

The authors declare no competing financial interests.

### ACKNOWLEDGMENT

The work is supported by the Shanxi Province International Cooperation Program (2014081004), the National Basic Research Program of China (No. 2011AA05A205), and the National Natural Science Foundation of China (91545109). QY appreciates the support from the research funding of Aston University. BX acknowledges the EPSRC for the support (EP/M027295/1).

## REFERENCES

- (1) Rosi, N. L.; Eckert, J.; Eddaoudi, M.; Vodak, D. T.; Kim, J.; O'Keeffe, M.; Yaghi, O. M., Hydrogen Storage in Microporous Metal-Organic Frameworks. *Science* 2003, 1127-1129.
- (2) Mitchell, L.; Gonzalez-Santiago, B.; Mowat, J. P. S.; Gunn, M. E.; Williamson, P.; Acerbi, N.; Clarke, M. L.; Wright, P. A., Remarkable Lewis Acid Catalytic Performance of The Scandium Trimesate Metal Organic Framework MIL-100(Sc) for C–C and C=N Bond-Forming Reactions. *Catal. Sci. Technol.* 2013, 3, 606-617.
- (3) Xiao, B.; Wheatley, P. S.; Zhao, X.; Fletcher, A.J.; Fox, S.; Rossi, A.G.; Megson, I.L.; Bordiga, S.; Regli, L.; Thomas, K. M.; Morris, R.E., High-Capacity Hydrogen and Nitric Oxide Adsorption and Storage in a Metal–Organic Framework. *J Am. Chem. Soc.* 2007, 129, 1203-1209.
- (4) Manna, K.; Zhang, T.; Carboni, M.; Abney, C. W.; Lin, W., Salicylaldimine-Based Metal–Organic Framework Enabling Highly Active Olefin Hydrogenation with Iron and Cobalt Catalysts. *J. Am. Chem. Soc.* 2014, 136, 13182-13185.
- (5) Tang, J.; Dong, W.; Wang, G.; Yao, Y.; Cai, L.; Liu, Y.; Zhao, X.; Xu, J.; Tan, L., Efficient Molybdenum(VI) Modified Zr-MOF Catalysts for Epoxidation of Olefins *RSC Adv.* 2014, 4, 42977-42982.
- (6) Dong, X.; Liu, T.; Hu, Y.; Liu, X.; Che, C., Urea Postmodified in A Metal–Organic Framework as A Catalytically Active Hydrogen-Bond-Donating Heterogeneous Catalyst. *Chem. Commun.* 2013, 49, 7681-7683.
- (7) Santos, V. P.; Wezendonk, T. A.; Jaén, J. J. D.; Dugulan, A. I.; Nasalevich, M. A.; Islam, H. U.; Chojecki, A.; Sartipi, S.; Sun, X.; Hakeem, A. A.; Koeken, A. C. J.; Ruitenbeek, M.; Davidian, T.; Meima, G. R.; Sankar, G.; Kapteijn, F.; Makkee, M.; Gascon, J., Metal Organic Framework-Mediated Synthesis of Highly Active and Stable Fischer-Tropsch Catalysts. *Nat. Commun.* 2015, 6, 6451-6458.
- (8) Wezendonk, T. A.; Santos, V.P.; Nasalevich, M. A.; Warringa, Q. S. E.; Dugulan, A. I.; Chojecki, A.; Koeken, A. C. J.; Ruitenbeek, M.; Meima, G.; Islam, H-U; Sankar, G.; Makkee, M.; Kapteijn, F.; Gascon, J., Elucidating the Nature of Fe Species during Pyrolysis of the Fe-BTC MOF into Highly Active and Stable Fischer–Tropsch Catalysts. *ACS Catal.* 2016, 6, 3236-3247.
- (9) Pei, Y.; Li, Z.; Li Y., Highly active and selective Co-based Fischer–Tropsch Catalysts Derived from Metal–Organic Frameworks. *AIChE J.* 2017, 63, 2935-2944.
- (10) Qiu, B.; Yang, C.; Guo, W.; Xu, Y.; Liang, Z.; Ma, D.; Zou, R. J., Highly Dispersed Co-Based Fischer–Tropsch Synthesis Catalysts from Metal–Organic Frameworks. *Mater. Chem. A* 2017, 5, 8081-8086.
- (11) Jagadeesh, R. V.; Murugesan, K.; Alshammari, A. S.; Neumann, H.; Pohl, M. M.; Radni, J; Beller, M., MOF-derived Cobalt Nanoparticles Catalyze a General Synthesis of Amines. *Science* 2017, 358, 326-332.
- (12) Sun, X.; Olivos-Suarez, A. I.; Meijerink, M.; van Deelen, T.; Ould-Chikh, S.; Zečević, J.; de Jong, K. P.; Kapteijn, F.; Gascon, J. Manufacture of Highly Loaded Silica-Supported Cobalt Fischer–Tropsch Catalysts from a Metal Organic Framework. *Nat. Commun.* 2017, 8, 1680.

- (13) Sun, X.; Olivos-Suarez A. I.; Oar-Arteta, L.; Rozhko, E.; Osadchii, D.; Bavykina, A.; Kapteijn, F.; Gascon, J., Metal-Organic Framework Mediated Cobalt/Nitrogen-Doped Carbon Hybrids as Efficient and Chemoselective Catalysts for the Hydrogenation of Nitroarenes. *ChemCatChem* 2017, 9, 1854-1862.
- (14) Dong, Z.; Le, X.; Liu, Y.; Dong, C.; Ma, J., Metal Organic Framework Derived Magnetic Porous Carbon Composite Supported Gold and Palladium Nanoparticles as Highly Efficient and Recyclable Catalysts for Reduction of 4-Nitrophenol and Hydrodechlorination of 4-Chlorophenol. *J Mater Chem A* 2014, 2, 18775-18785.
- (15) Dong, W.; Zhang, L.; Wang, C.; Feng, C.; Shang, N.; Gao, S.; Wang, C., Palladium Nanoparticles Embedded in Metal–Organic Framework Derived Porous Carbon: Synthesis and Application for Efficient Suzuki–Miyaura Coupling Reactions. *Rsc Adv.* 2016, 6, 37118-37123.
- (16) Liu, J. X.; Su, H. Y.; Sun, D. P.; Zhang, B. Y.; Li, W. X., Crystallographic Dependence of CO Activation on Cobalt Catalysts: HCP versus FCC. *J. Am. Chem. Soc.* 2013, 135, 16284-16287.
- (17) Mohandas, J. C.; Gnanamani, M. K.; Jacobs, G.; Ma, W. P.; Ji, Y.; Khalid, S.; Davis, B. H., Fischer–Tropsch Synthesis: Characterization and Reaction Testing of Cobalt Carbide. *ACS Catal.* 2011, 1, 1581-1588.
- (18) Bezemer, G. L.; Bitter, J. H.; Kuipers, H. P.; Oosterbeek, H.; Holewijn, J. E.; Xu, X.; Kapteijn, F.; van Dillen, A. J.; de Jong, K. P., Cobalt Particle Size Effects in the Fischer–Tropsch Reaction Studied with Carbon Nanofiber Supported Catalysts. *J. Am. Chem. Soc.* 2006, 128, 3956-3964.
- (19) Anderson, R. B. *The Fischer-Tropsch Synthesis*. Academic Press, Orlando 1984.
- (20) Kogelbauer, A.; Weber, J. C.; Goodwin Jr., J. G., The Formation of Cobalt Silicates on Co/SiO<sub>2</sub> Under Hydrothermal Conditions. *Catal. Lett.* 1995, 34, 259-267.
- (21) Wilcoxon, J. P.; Abrams, B. L., Synthesis, Structure and Properties of Metal Nanoclusters. *Chem. Soc. Rev.* 2006, 35, 1162-1194.
- (22) Barbier, A.; Tuel, A.; Arcon, I.; Kodre, A.; Martin, G. A., Characterization and Catalytic Behavior of Co/SiO<sub>2</sub> Catalysts: Influence of Dispersion in the Fischer–Tropsch Reaction. *J. Catal.* 2001, 200, 106-116.
- (23) Ho, S. W.; Houalla, M.; Hercules, M. D., Effect of Particle Size on Carbon Monoxide Hydrogenation Activity of Silica Supported Cobalt Catalysts. *J. Phys. Chem.* 1990, 94, 6390-6399.
- (24) Iglesia, E.; Soled, S. L; Fiato, R. A., Fischer-Tropsch Synthesis on Cobalt and Ruthenium. Metal Dispersion and Support Effects on Reaction Rate and Selectivity. *J. Catal.* 1992, 137, 212-224.
- (25) Prieto, G.; Martínez, A.; Concepción, P.; Moreno-Tost, R., Cobalt Particle Size Effects in Fischer–Tropsch Synthesis: Structural and in Situ Spectroscopic Characterisation on Reverse Micelle-Synthesised Co/ITQ-2 Model Catalysts. *J. Catal.* 2009, 266,129-144.
- (26) Breejen, J. P. den; Radstake, P. B.; Bezemer, G. L.; Bitter, J. H.; Frøseth, V.; Holmen, A.; de Jong, K. P., On the Origin of the Cobalt Particle Size Effects in Fischer–Tropsch Catalysis. *J Am. Chem. Soc.* 2009, 131, 7197-7203.

- (27) Chen, L.; Wang, C.; Chen, G., Synthesis of Carbon Onions Including Fe<sub>3</sub>C by Chemical Vapor Deposition Using an Iron Catalyst Supported on Sodium Chloride. *Appl. Mech. Mater.* 2012, 184-185, 1294-1297.
- (28) Fazle Kibria, A. K. M.; Mo, Y. H.; Nahm, K. S.; Kim, M. J., Synthesis of Narrow-Diameter Carbon Nanotubes from Acetylene Decomposition over an Iron–Nickel Catalyst Supported on Alumina. *Carbon* 2002, 40, 1241-1247.
- (29) Lian, W.; Song, H.; Chen, X.; Li, L.; Huo, J.; Zhao, M.; Wang, G., The Transformation of Acetylene Black Into Onion-Like Hollow Carbon Nanoparticles at 1000°C Using an Iron Catalyst. *Carbon* 2008, 46, 525-530.
- (30) Karthikeyan, S.; Mahalingam, P., Karthik, M. Large Scale Synthesis of Carbon Nanotubes. *E–J. Chem.* 2009, 6, 1-12.
- (31) Miao, J.; Kuppala D. W. H.; Narasimhulu, V.; Lin, P.; Chen, Y.; Hwang, L., Synthesis and Properties of Carbon Nanospheres Grown by CVD using Kaolin Supported Transition Metal Catalysts. *Carbon* 2004, 42, 813-822.
- (32) Liu, T.; Liu, Y., Synthesis of Carbon Nanocapsules and Carbon Nanotubes by an Acetylene Flame Method. *Carbon* 2006, 44, 2045-2050.
- (33) Dietzel, P.D.C.; Morita, Y.; Blom, R.; Fjellvag, H., An In Situ High-Temperature Single-Crystal Investigation of a Dehydrated Metal–Organic Framework Compound and Field-Induced Magnetization of One-Dimensional Metal–Oxygen Chains. *Angew. Chem. Int. Ed.* 2005, 44, 6354-6358.
- (34) Glover, T. G.; Peterson, G. W.; Schindler, B. J.; Britt, D.; Yaghi, O., MOF-74 Building Unit Has a Direct Impact on Toxic Gas Adsorption. *Chem. Eng. Sci.* 2011, 66, 163-170.
- (35) Xu, J.; Yang, Y.; Li, Y. Recent Development in Converting Coal to Clean Fuels in China. *Fuel* 2015, 152, 122-130.
- (36) Hu, J.; Yu, F.; Lu Y., Application of Fischer–Tropsch Synthesis in Biomass to Liquid Conversion. *Catalysts* 2012, 2, 303-326.
- (37) Leckel, D., Diesel Production from Fischer–Tropsch: The Past, the Present, and New Concepts. *Energy Fuels* 2009, 23, 2342-2358.
- (38) Díaz, J. A.; Akhavan, H.; Romero, A.; Garcia-Minguillan, A. M.; Romero, R.; Giroir-Fendler, A.; Valverde, J. L., Cobalt and Iron Supported on Carbon Nanofibers as Catalysts for Fischer–Tropsch Synthesis. *Fuel Process. Technol.* 2014, 128, 417-424.
- (39) Zhai, P.; Xu, C.; Gao, R.; Liu, X.; Li, M.; Li, W.; Fu, X.; Jia C.; Xie J.; Zhao, M., Wang X.; Li, Y.; Zhang, Q., Highly Tunable Selectivity for Syngas-Derived Alkenes over Zinc and Sodium-Modulated Fe<sub>5</sub>C<sub>2</sub> Catalyst. *Angew. Chem. Int. Ed.* 2016, 55, 9902-9907.
- (40) Xiong, H.; Motchelaho, M.; Moyo, M.; Jewell, L. L.; Coville, N. J., Correlating the Preparation and Performance of Cobalt Catalysts Supported on Carbon Nanotubes and Carbon Spheres in the Fischer–Tropsch Synthesis. *J. Catal.* 2011, 278, 26-40.
- (41) Li, H. B.; Yue, Q. L.; Xu, S. L.; Wang, L.; Liu, J. F., Fabrication of Octahedral Carbon Nanocages via an In-situ Template Approach. *Mater. Lett.* 2012, 66, 353-356.

- (42) Moen, A.; Nicholson, D. G., X-ray Absorption Spectroscopic Studies at the Cobalt K-Edge on a Reduced Al<sub>2</sub>O<sub>3</sub>-Supported Rhenium-Promoted Cobalt Fischer–Tropsch Catalyst. *Chem. Mater.* 1997, 9, 1241-1247.
- (43) Lizárraga, R.; Pan, F.; Bergqvist, L.; Holmström, E.; Gercsi, Z.; Vitos, L., First Principles Theory of the hcp-fcc Phase Transition in Cobalt. *Scientific Reports* 2017, 7, 3778, 1-7.
- (44) Zhao, Z. Q.; Veintemillas-Verdaguer, S.; Bormati-Miguel, O.; Morales, M. P.; Xu, H. B., Thermal History Dependence of the Crystal Structure of Co Fine Particles. *Phys. Rev. B* 2005, 71, 024106.
- (45) Takenaka, S.; Orita, Y.; Matsune, H.; Tanabe, E.; Kishida, M., Structures of Silica-Supported Co Catalysts Prepared Using Microemulsion and Their Catalytic Performance for the Formation of Carbon Nanotubes through the Decomposition of Methane and Ethylene. *J. Phys. Chem. C* 2007, 111, 7748-7756.
- (46) Morales, F.; Grandjean, D.; Mens, A.; de Groot, F. M. F.; Weckhuysen, B. M., X-ray Absorption Spectroscopy of Mn/Co/TiO<sub>2</sub> Fischer–Tropsch Catalysts: Relationships between Preparation Method, Molecular Structure, and Catalyst Performance. *J. Phys. Chem. B* 2006, 110, 8626-8639.
- (47) Fu, T.; Lv, J.; Li, Z., Effect of Carbon Porosity and Cobalt Particle Size on the Catalytic Performance of Carbon Supported Cobalt Fischer–Tropsch Catalysts. *Ind. Eng. Chem. Res.* 2014, 53, 1342-1350.
- (48) Xie, W.; Zhang, Y.; Liew, K.; Li, J., Effect of Catalyst Confinement and Pore Size on Fischer-Tropsch Synthesis over Cobalt Supported on Carbon Nanotubes. *Sci. China: Chem.* 2012, 55(9): 1811-1816.
- (49) Huang, J.; Qian, W.; Ma, H.; Zhang, H.; Ying, W., Highly Selective Production of Heavy Hydrocarbons over Cobalt–Graphene–Silica Nanocomposite Catalysts. *RSC Adv.* 2017, 7: 33441-33449.
- (50) Huang, J.; Qian, W.; Ma, H.; Zhang, H.; Ying, W., Cobalt Supported on Graphene – A Promising Novel Fischer–Tropsch Synthesis Catalyst. *Appl. Catal., A* 2015, 499, 188-196.
- (51) Cheng, K.; Subramanian, V.; Carvalho, A.; Ordonsky, V. V.; Wang, Y.; Khodakov, A. Y., The Role of Carbon Pre-coating for the Synthesis of Highly Efficient Cobalt Catalysts for Fischer–Tropsch Synthesis. *J. Catal.* 2016, 337, 260-271.
- (52) Karaca, H.; Safonova, Q. V.; Chambrey, S.; Fongarland, P.; Roussel, P.; Griboval-Constant, A.; Lacroix, M.; Khodakov, A. Y., Structure and Catalytic Performance of Pt-Promoted Alumina-Supported Cobalt Catalysts Under Realistic Conditions of Fischer–Tropsch Synthesis. *J. Catal.* 2011, 277, 14-26.
- (53) Ducreux, O.; Lynch, J.; Rebours, B.; Roy, M.; Chaumette, P., In Situ Characterization of Cobalt Based Fischer-Tropsch Catalysts: A New Approach to the Active Phase. *Stud. Surf. Sci. Catal.* 1998, 119, 125-130.
- (54) Enache, D.I.; Rebours, B.; Roy-Auberger, M.; Fierro, R.J., In Situ XRD Study of the Influence of Thermal Treatment on the Characteristics and the Catalytic Properties of Cobalt-Based Fischer–Tropsch Catalysts. *J. Catal.* 2002, 205, 346-353.
- (55) de la Peña O'Shea, V.A.; Homs, N.; Fierro, J. L.G.; Ramírez de la Piscina, P., Structural Changes and Activation Treatment in a Co/SiO<sub>2</sub> Catalyst for Fischer-Tropsch Synthesis. *Catal. Today* 2006, 114, 422-427.

- (56) Gnanamani, M.K.; Jacobs, G.; Shafer, W. D.; Davis, B. H., Fischer–Tropsch Synthesis: Activity of Metallic Phases of Cobalt Supported on Silica. *Catal. Today* 2013, 215, 13-17.
- (57) Khodakov, A. Y.; Chu, W.; Fongarland, P., Advances in the Development of Novel Cobalt Fischer–Tropsch Catalysts for Synthesis of Long-Chain Hydrocarbons and Clean Fuels. *Chem. Rev.* 2007, 107, 1692-1744.
- (58) Chen, W.; Fan, Z.; Pan, X.; Bao, X., Effect of Confinement in Carbon Nanotubes on the Activity of Fischer–Tropsch Iron Catalyst. *J. Am. Chem. Soc.* 2008, 130(29): 9414-9419.
- (59) Chen, W.; Pan, X.; Bao, X., Tuning of Redox Properties of Iron and Iron Oxides via Encapsulation within Carbon Nanotubes. *J. Am. Chem. Soc.* 2007, 129, 7421-7426.
- (60) Melaet, G.; Ralston, W. T.; Li, C.; Alayoglu, S.; An, K.; Musselwhite, N.; Kalkan, B. and Somorjai, G. A., Evidence of Highly Active Cobalt Oxide Catalyst for the Fischer–Tropsch Synthesis and CO<sub>2</sub> Hydrogenation. *J. Am. Chem. Soc.* 2014, 136 (6), 2260-2263.